Journal of Theoretical Biology 282 (2011) 41–51

Contents lists available at ScienceDirect

Journal of Theoretical Biology

journal homepage: www.elsevier.com/locate/yjtbi

Elastic instability model of rapid beak closure in hummingbirds

M.L. Smith [a,*,1], G.M. Yanega [b,1,2], A. Ruina [a]

[a] Department of Theoretical and Applied Mechanics, Cornell University, Ithaca, NY 14853, United States
[b] Department of Ecology and Evolutionary Biology, University of Connecticut, Storrs, CT 06269, United States

ARTICLE INFO

Article history:
Received 2 December 2010
Received in revised form
4 May 2011
Accepted 6 May 2011
Available online 18 May 2011

Keywords:
Functional morphology
Avian feeding mechanics
Physical models
Insectivory
Trochilidae

ABSTRACT

The hummingbird beak, specialized for feeding on floral nectars, is also uniquely adapted to eating flying insects. During insect capture the beak often appears to close at a rate that cannot be explained by direct muscular action alone. Here we show that the lower jaw of hummingbirds has a shape and compliance that allows for a controlled elastic snap. Furthermore, hummingbirds have the musculature needed to independently bend and twist the sides of the lower jaw. According to both our simple physical model and our elastic instability calculation, the jaw can be smoothly opened and then snapped closed through an appropriate sequence of bending and twisting actions by the muscles of the lower jaw.

1. Introduction

It is often assumed that specialization for nectar feeding drives the evolution of structural and physiological traits in hummingbirds (Aves: Trochilidae) (Suarez, 1998; Temeles and Kress, 2003). Yet, because the nectars hummingbirds consume lack sufficient nutrients, they must augment their diet by consuming insects and other arthropods (Baker and Baker, 1982). These birds obtain the majority of their prey by flying from a perch to snatch small insects in flight (Stiles, 1995). Most aerial insectivores, unlike hummingbirds, possess broad beaks and large gapes (mouth openings) (Zweers et al., 1994). Hummingbirds appear able to circumvent the functional trade-off between nectar and insect consumption by increasing the width of the gape at the base of the jaws via flexion of the mandible (lower jaw) (Yanega and Rubega, 2004).

In general, lateral (sideways) flexion of the lower jaw increases the effective size of the gape and has two primary modes of expression among birds. The first form aids with the transport of large food items from the beak to the esophagus (Zusi, 1993; Lee et al., 1999; Gibb et al., 2008). A characteristic of this motion is that the upper jaw is in its closed position and the lower jaw structure spreads laterally (Zusi and Warheit, 1992). The second kind of intramandibular flexion is used solely to capture prey while both jaws are open and apart. This jaw distortion is found primarily in a clade of ancient aerial insectivores, the Cypselomorphae, including hummingbirds, swifts, tree-swifts, owlet-nightjars, nightjars, and potoos (Bühler, 1970; Mayr, 2005) (Fig. 1).

All birds who flex their mandibles laterally possess a bending zone near the tip of the beak (anterior) and one toward the base of the jaw (posterior). Typically, the anterior zone features reduced calcification and thinning of the bone (Meyers and Myers, 2005). The posterior bending zone features a hinge composed of cartilage, thin plate springs, or a synovial capsule that joins the posterior mandibular bones to those in front of the hinge (Bühler, 1981; Zusi and Warheit, 1992). Hummingbirds, however, differ from all other birds (Fig. 1) in that their posterior bending zone consists of thin, continuous bone.

This continuous bending zone features an elongated cross section that is more stiff for bending in one direction than in the orthogonal direction.

The flexibility and shape of the hummingbird mandible leads to uncommon functional consequences. Hummingbird mandibular flexion includes a side-to-side (mediolateral) spreading of the mandible followed by a smooth dipping (dorsoventral flexion) of the anterior portion of the lower jaw. This complex flexion is observed when hummingbirds attempt to catch flying insects (Fig. 2). Additionally, due to the coupling between the lateral and dorsoventral flexion, hummingbirds appear able to use a controlled elastic instability to rapidly snap their lower jaw from the

* Corresponding author. Present address: Nanostructured and Biological Materials Branch, Materials and Manufacturing Directorate, Air Force Research Laboratory, WPAFB, OH, USA.
E-mail addresses: mls238@cornell.edu, matthew.smith.ctr@wpafb.af.mil (M.L. Smith).
[1] These authors contributed equally to this work.
[2] Present address: National Evolutionary Synthesis Center, 2024 W. Main Street, Suite A200, Durham, NC 27705, USA.

0022-5193/$ - see front matter © 2011 Elsevier Ltd. All rights reserved.
doi:10.1016/j.jtbi.2011.05.007

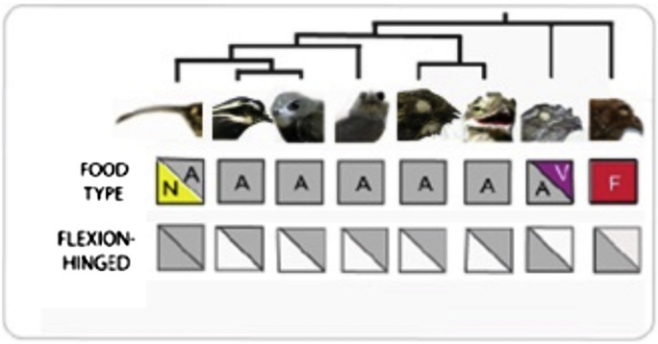

Fig. 1. Hummingbirds are unique among avian insectivores, exhibiting mandibular flexion without a hinge in the posterior flexion zone. The lower line indicates whether or not birds in a family are known to flex their mandible when feeding (gray in the upper right corner of the box). Those with a hinge are shown white in the lower left side of the box; gray indicates the lack of any hinge. Diet types indicated in the upper line are coded N=nectar; A=arthropods; V=vertebrates; and F=fruit. At the top are displayed the phylogenetic relationships among clades of ancient insectivores (after Mayr, 2009). The avian families included in the Cypselomorphae group are pictured from left to right: Trochilidae (hummingbirds); Hemiprocnidae (tree-swifts); Apodidae (swifts); Aegothelidae (owlet-nightjars); Caprimulgidae (nighthawks); and Nyctibiidae (potoos). The remaining two families, Podargidae (frogmouths) and Steatornithidae (oilbirds), combine with the aforementioned families to form a clade known as Strisores.

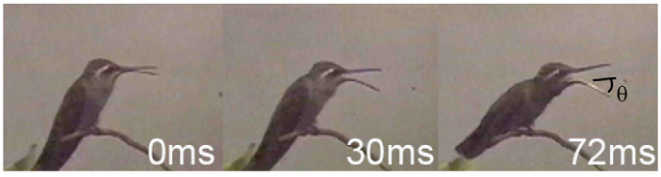

Fig. 2. A blue-throated hummingbird's (*Lampornis clemenciae*) beak opens and bends downward during attempted insect capture. Shown with measured dorsoventral flexion of $\theta \approx 27^{\circ}$.

flexed position to the straight position. This action is perhaps similar to the snapping of a toggle switch. Observed variation in the degree of flexion in response to insect position, and independent movement of the upper and lower jaws, suggests that (1) the movement of the upper and lower jaws is largely uncoupled and (2) mandibular flexion is under active muscular control.

Examples of rapid elastic energy release in nature are common. In botany elastic instabilities might be categorized as snap-buckling or explosive fracture (Skotheim and Mahadevan, 2005). Explosive fracture is analogous to the non-reversible release of a cocked catapult and is used, for example, by plants for seed or pollen dispersal (Taylor et al., 2006; Hayashi et al., 2009). In the animal kingdom "explosive" elastic energy release by some trigger mechanism is relatively common for both predation and locomotion (Bennet-Clark and Lucey, 1967; Gronenberg, 1995; de Groot and van Leeuwen, 2004; Van Wassenbergh et al., 2008; Zack et al., 2009). One example of snap-buckling in plants is the snapping leaves of the venus flytrap (Forterre et al., 2005). The driving parameter of the macroscopic snap appears to be a change in the natural curvature of the leaf resulting from fluid flow triggered by hairs located on the leaf's inner surface. After the leaves have closed and once the prey has been digested, the leaves can smoothly return to their reference state where they are in a position to snap again. Snap-buckling is also used by some insects, e.g. the cicada, to produce sound (Young and Bennet-Clark, 1995; Skals and Surlykke, 1999; Bennet-Clark and Daws, 1999). Whereas the cicada buckles in two directions the venus flytrap has a snap and a smooth return. The hummingbird beak snap seems analogous to the snap and smooth return seen in the venus flytrap.

Here we estimate the power necessary to swing the beak closed by modeling the mandible as a straight, rigid bar pinned at one end (i.e., with no mid-mandible flexion). The power to rotate such a bar about the pin is $P=(1/3)mL\dot{\theta}\ddot{\theta}$, where m is the mass of the bar, L is the length, $\dot{\theta}$ is the angular velocity, and $\ddot{\theta}$ is the angular acceleration. We measured beak tip displacements with high speed video (Yanega, unpublished data; see also Appendix A). The maximum instantaneous power density generally ranged from 270 to 770 W kg^{-1}. The power output of flight muscles during maximal loading for similarly sized hummingbirds has been reported to be 309 W kg^{-1} (Chai and Millard, 1997). In reality, the hummingbird mandible is not a rigid bar but is visibly flexed. We noted that the flexed anterior portion of the mandible rotated through approximately 11° in approximately 2 ms, an angular velocity of nearly 5500° per second. Because the power required is generally greater than the maximum power known for hummingbird muscles it seems unlikely that direct muscular action can be solely responsible for the rapid snap-closure. Our proposal here is that this rapid motion can be explained as a controlled elastic instability. Other than the hummingbirds we present here, we are aware of no other vertebrates that use snap-buckling for predation or locomotion. In what follows we demonstrate a method (based on video evidence, anatomical inference, and a simple mechanical model) by which the hummingbird may smoothly flex its mandible laterally and dorsoventrally, store elastic energy, and then by precise control of its muscles produce a sudden snap.

2. Physical model

2.1. Hummingbird mandible structure

The mandible is composed of two branching bones, the rami, which form a fused junction or symphysis at the tip of the jaw. The symphysis is typically short (2–4 mm) in most hummingbirds, and the mandible is capable of flexion just prior to it at decalcified bending zones (Meyers and Myers, 2005). The middle of the rami, anterior to the mandibular fenestra (the hole at 2 in Fig. 3), is elongated, thin, and compressed. It is thickened on the upper and lower rims of the jaw while thinner in the middle (Fig. 3, cross section 1), resembling an I-beam in construction

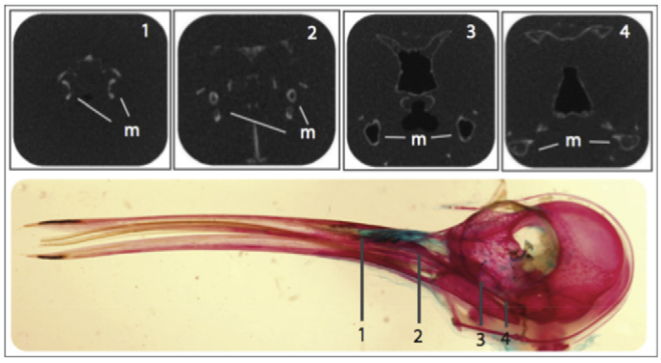

Fig. 3. An elongated mandible cross section near the posterior flexion zone at slice 1 allows for compliant horizontal bending and resists vertical bending. The mandible is indicated by the letter m. Shown is a lateral view of a cleared and stained hummingbird skull (red, bone; blue, cartilage) with cross sections at four locations. Solid bone in the cross sections is depicted by the color white and hollow space is shown in black. The hollow cross sections (2, 3, and 4) are relatively stiff in all directions. Total length of the mandible is approximately 27 mm, and cross section 2 is approximately 1.5 mm high and 0.5 mm wide. (For interpretation of the references to color in this figure legend, the reader is referred to the web version of this article.)

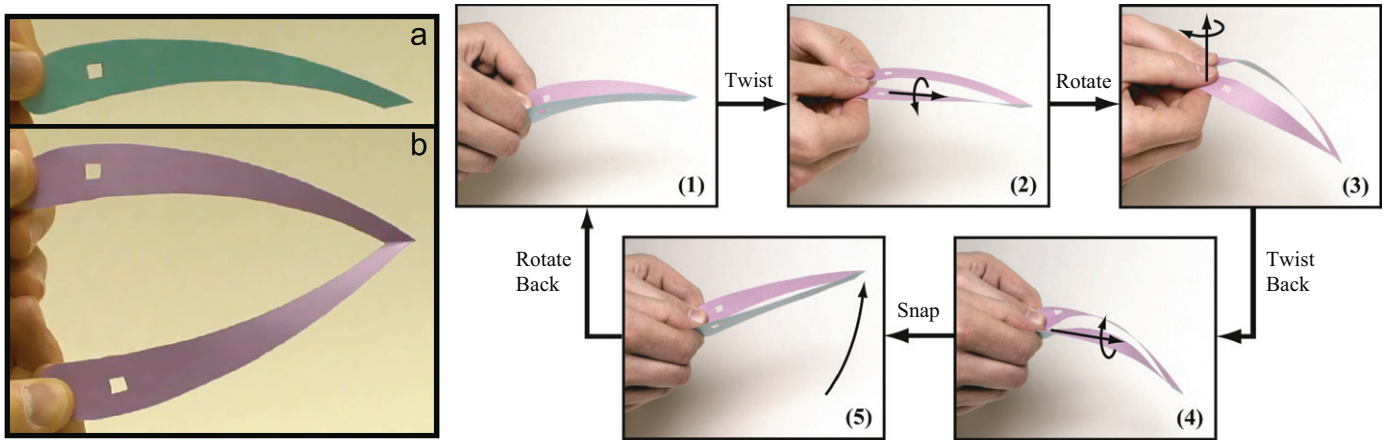

Fig. 4. Model of a hummingbird mandible cut from a piece of paper with a single fold. The beak tip is reproduced by the small portion of the fold which is left intact. A hole for the fenestra is present as a reference, but does not affect the model performance. (a) Side view (folded flat). (b) Top view (opened up). (1)–(5) Flexion and snap sequence produced by twisting and rotating the base of the paper mandible. (1) Reference configuration. (2) The rami are twisted out. (3) The rami are rotated out while twist is maintained. (4) The rotation is held fixed while the rami are partially twisted back. The paper mandible snaps between panels (4) and (5). (5) The rami remain rotated out. Rotating the rami back returns the model to the reference configuration.

(Bock and Kummer, 1968). The shape of this cross section makes it particularly flexible about its long axis and relatively stiff about the corresponding perpendicular axis. In other words, the structure of the cross section makes the mandible more compliant to outward bending than vertical bending (as viewed in the resting position). The posterior portion of the mandible is pneumatic (containing air), cancellous, and inflexible (Fig. 3, cross section 3). The kinetics and musculature involved in intramandiblular flexion will be discussed further in Section 6.

2.2. Paper model

We constructed a paper model to mimic both the shape and flexibility of the hummingbird lower jaw (Fig. 4). It is important to note that long, thin structures having *cross sections* that feature aspect ratios (long dimension divided by short dimension) of three to four will display qualitatively similar bending compliance to a structure with cross sections having much larger aspect ratios. Therefore, a key feature of the paper model is its elongated cross section. Though the aspect ratio is extreme compared to the hummingbird mandible, it produces a qualitatively similar compliance. Fig. 4 illustrates that the base of the model rami can be manipulated to imitate the smooth flexion and apparent snap-buckling in hummingbirds. We use the word "twist" to refer exclusively to rotation about the longitudinal axis of the rami (as in Fig. 4 from (1) to (2)), and the term "rotate" to refer to rotations about the vertical axis running through the posterior end of the rami (as in Fig. 4 from (2) to (3)). The model begins in a relaxed reference configuration, Fig. 4 (1), and proceeds through the following sequence:

(1) → (2), *Twist*: The rami are twisted out about their long axes, which orient the flat surface dorsoventrally and result in a small amount of dorsoventral flexion.
(2) → (3), *Rotate*: The dorsoventral flexion is magnified when the twist is maintained and the rami are rotated out laterally.
(3) → (4), *Twist back*: The rami are twisted back about their longitudinal axes toward the reference configuration while the rotation from (3) is held fixed. This step moves the mandible toward an elastic instability where it will snap into a straightened position. In the hummingbird the snap is accompanied by the additional motion of the entire mandible pivoting about its base to a closed position.
(4) → (5), *Snap*: In (5) the mandible is shown just after the snap with the rami still rotated out. It appears that the mandible is pointing up slightly but this is only an artifact of the manner in which the model must be held in the fingers.
(5) → (1), *Rotate back*: The rami are rotated back to the reference configuration.

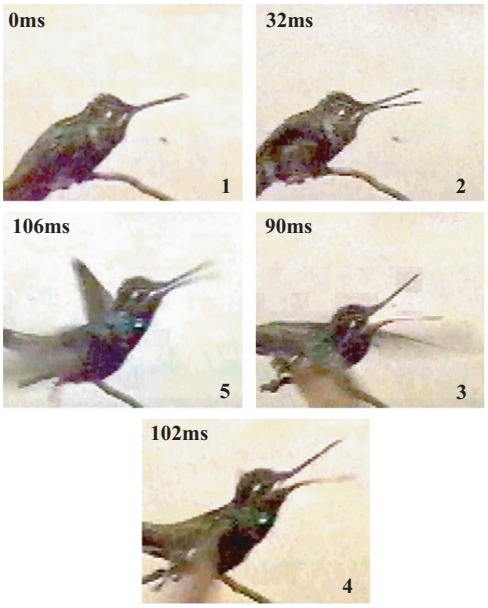

Fig. 5. Flexion sequence of the hummingbird mandible during insect capture. Based on the proposed flexion-snap sequence in the paper model the actions in each panel are: (1) reference configuration; (2) the rami are twisted out; (3) the rami are rotated out while the twist is held constant; (4) the rami are twisted back while the rotation is held fixed; (5) the mandible pivots shut while simultaneously undergoing snap-buckling. Note the short time interval between frames (4) and (5).

The extended loading period and rapid snap closure exhibited by the paper model mirrors the motion of the hummingbird beak seen in video (Fig. 5). In panel (2) the hummingbird displays its

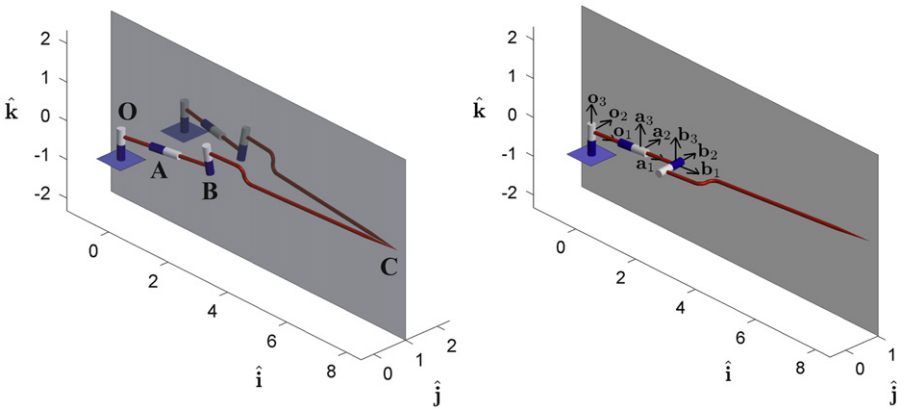

Fig. 6. (a) Rigid bar model of a hummingbird mandible shown with a vertical plane through the medial-axis. Hinges *A* and *B* mimic torsion and bending in the posterior (mid-rami) flexion zone, respectively. Hinge *O* mimics lateral rotations at the base of the rami. (b) Half of the rigid bar model is shown with the attached moving bases $\{\mathbf{o}_i\}$, $\{\mathbf{a}_i\}$, and $\{\mathbf{b}_i\}$. The angles of rotation are as follows: θ_1 gives rotations about the $\mathbf{a}_1$ axis, θ_2 gives rotations about $\mathbf{b}_2$, and θ_3 gives rotations about $\mathbf{o}_3$. Lengths not to scale. (For interpretation of the references to color in this figure legend, the reader is referred to the web version of this article.)

ability to control flexion by dipping its mandible while the jaw is still closed. Dorsoventral flexion of both the upper and lower jaws is clearly visible in panel (3). This dual flexion likely results in considerable antagonism between the muscle groups responsible for opening and closing the jaws. Rapid closure is on display from panel (4) to just after panel (5), taking approximately 6 ms. We note that panel (5) in Fig. 5 corresponds to the period between steps (4) and (5) in Fig. 4.

3. Mathematical formulation

We postulate a simple mathematical model (Fig. 6) of both the hummingbird and the paper jaw.

The model is based on the mechanics of rigid rods interconnected by hinges with torsional springs. The torsional springs resist rotation of the gray cylinders with respect to the dark blue cylinders. Hinge *B* is aligned with the elongated axis of the bone cross section in the posterior flexion zone (cf. Fig. 3, Section 1). As a result, deformation at hinge *B* represents bending of the mandible in the most compliant direction in the posterior flexion zone. Similarly, hinge *A* represents torsion of the bone in the posterior flexion zone. Finally, hinge *O* accounts for lateral rotation at the mandible base.

The model is reflection symmetric about the medial-axis of the jaw as indicated by the dark gray vertical plane. The tip is constrained to frictionless motion within the plane, and due to the symmetry we restrict the analysis to a single side of the model mandible. A normal force corresponding to an internal force in the jaw tip is required to maintain the plane constraint on the model tip. Naturally, the anterior flexion zone will also resist moments. However, we suggest that the features of the model already introduced are the most important for explaining the flexion-snap phenomenon.

We represent applied rotations of the rami by introducing a spring bias, α, in hinge *O* (i.e., if hinge *O* were allowed to rotate freely, α would specify its orientation). We model applied mandibular twisting by introducing a second spring bias, ω, in hinge *A*. We refer to α as the rotation bias and to ω as the twist bias. The biases emulate muscular action on the jaw bone, and can be thought of as user controlled parameters in the model.

Let $\mathcal{K}_1$, $\mathcal{K}_2$, and $\mathcal{K}_3$ designate the stiffnesses of the springs in hinges *A*, *B*, and *O*, respectively. Using static balance of moments, three equilibrium equations along with the plain constraint, *p*, can be written as follows (see Appendix B for details):

$$\mathcal{K}_1(\omega-\theta_1)-\lambda L_{BC}\cos\vartheta_1\sin\vartheta_2\cos\vartheta_3=0, \tag{3.1}$$

$$-\mathcal{K}_2(\theta_2)+\lambda L_{BC}\sin\vartheta_2\sin\vartheta_3-\lambda L_{BC}\sin\vartheta_1\cos\vartheta_2\cos\vartheta_3=0, \tag{3.2}$$

$$\mathcal{K}_3(\alpha-\theta_3)-\lambda L_{OB}\cos\vartheta_3-\lambda L_{BC}\cos\vartheta_2\cos\vartheta_3+\lambda L_{BC}\sin\vartheta_1\sin\vartheta_2\sin\vartheta_3=0, \tag{3.3}$$

$$p(\theta_1,\theta_2,\theta_3)=0, \tag{3.4}$$

where θ_1 is the angle of rotation about $\mathbf{a}_1$, θ_2 is the angle of rotation about $\mathbf{b}_2$, θ_3 is the angle of rotation about $\mathbf{o}_3$, λ is the normal force at the tip, L_{OB} and L_{BC} are, respectively, the lengths from *O* to *B* and from *B* to *C*, and ϕ_1, ϕ_2, and ϕ_3 specify the orientation of the hinges in the reference configuration. Though the model is discreet, the reference configuration captures the basic form and position of the hummingbird mandible at rest. To simplify notation we also set $\vartheta_1=\phi_1+\theta_1$, $\vartheta_2=\phi_2+\theta_2$, and $\vartheta_3=\phi_3+\theta_3$. The positive direction of rotation as viewed from the head of the axis of rotation is counterclockwise. In keeping with the terminology of the previous section we refer to θ_1 as mandible twist or simply twist. We refer to θ_3 as mandible rotation or rotation, and θ_2 as flex. The mandible rotation provides a prediction of lateral mandibular spreading during insect capture, while the flex provides a prediction of the extent of dorsoventral flexion. Given the user controlled biases (α and ω) and the model parameters L_{OB}, L_{BC}, ϕ_1, ϕ_2, ϕ_3 , $\mathcal{K}_1$, $\mathcal{K}_2$, and $\mathcal{K}_3$, Eqs. (3.1)–(3.4) are sufficient to solve numerically for the four unknowns θ_1, θ_2, θ_3, and λ.

4. Model parameter values

To determine the bone lengths, reference angles, and spring stiffnesses, we require detailed knowledge of material properties and geometric dimensions of the hummingbird mandible. Because these properties are not readily available in the literature, we use a variety of sources to estimate the model parameters (see Appendix C and Smith (2009)). Geometric measurements are taken from available specimens with mandible and skull lengths comparable to the hummingbirds observed by Yanega and Rubega (2004). In addition, we utilize bone material properties from other species that exhibit flexibility similar to the hummingbird.

After initial estimates, we analyze numerical solutions of Eqs. (3.1)–(3.4) to tune final values for the model parameters. We judge the numerical findings by two primary criteria. First, the model configurations must qualitatively match the observed hummingbird mandible deformations, with physically reasonable values for the biases and mandible twist, rotation, and flex. Second, the maximum value of the flex (θ_2) should approach the flexion angle, 27°, measured from high speed video frames. During initial numerical investigation, the simplest parameters to obtain (L_{OB}, L_{BC}, ϕ_1, ϕ_2, ϕ_3, and $\mathcal{K}_2$) were held fixed while $\mathcal{K}_1$ and $\mathcal{K}_3$ were allowed to vary. Good numerical results, which we present in the next section, are obtained using the parameter values summarized in Table 1.

Table 1
Final estimates for the model parameters used in Eqs. (3.1)–(3.4).

Parameter	Value
L_{OB}	11 mm
L_{BC}	14 mm
$\mathcal{K}_1$	5.0×10^{-4} N mm
$\mathcal{K}_2$	9.6×10^{-4} N mm
$\mathcal{K}_3$	2.0×10^{-2} N mm
ϕ_1	$-79°$
ϕ_2	6°
ϕ_3	8°

5. Numerical results

We use the parameters given in Table 1 to numerically solve the set of nonlinear algebraic equations (3.1)–(3.4) for equilibrium configurations. Solutions for the flexion angle θ_2 form a folded surface, and we demonstrate a path by which the model flexes smoothly before losing stability and jumping to a stable equilibrium (Fig. 7). Though simple, the mechanical treatment presented in this work provides a good initial estimate of mandibular deformations and the energy stored during flexion.

Near the resting configuration, a suitable range of the two bias coordinates or controls (ω, α) was explored in order to reveal a folded surface. The vertical axis of the folded surface (Fig. 7a) gives the flex of the mandible. In Fig. 7b the surface is projected onto the $\omega-\alpha$ plane where a distinct cusp (a point where two curves meet) is easily recognized. A schematic representing the mandible configuration (the ball) on an energy landscape is given in Fig. 7c. The surface layer in between the folds represents unstable equilibria, i.e., the stored energy is locally maximized. Thus the mandible will not physically maintain this configuration and will move to one with a lower energy. One possible flexion-snap path is given by the sequence (1)–(5), where the labels correspond to the deformations of the paper model shown in Fig. 4. The desire to emulate the deformations observed in hummingbirds guides the specific numerical values of ω and α that make up a given flexion-snap path. The thick dashed line shows a jump from point (4) down to the lower "shelf" of the surface.

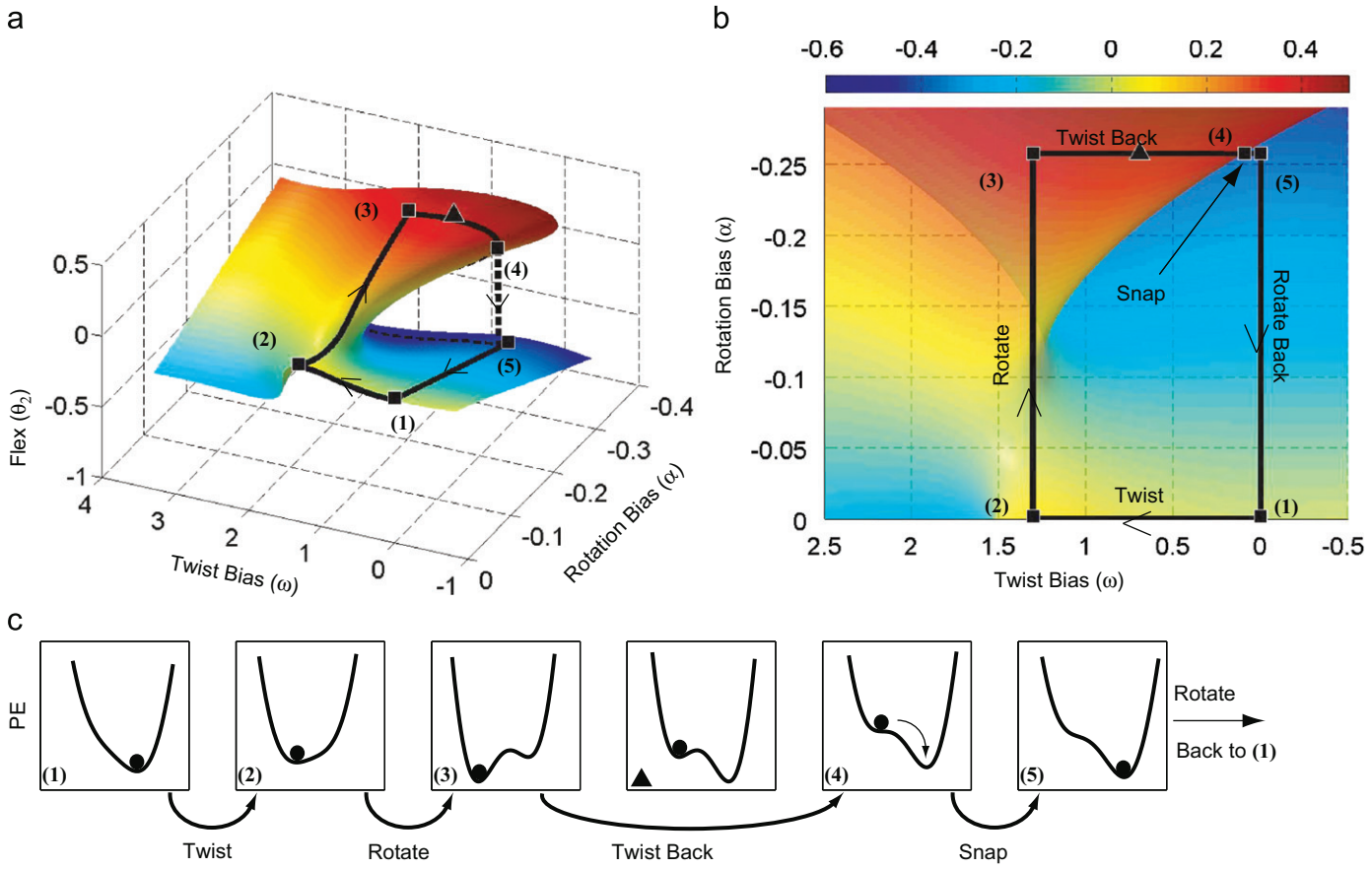

Fig. 7. (a) Folded surface of equilibrium solutions for the rigid bar model. The vertical axis is a measure of the rotation in hinge B. One possible flexion-snap path is shown on the surface. The solid black lines represent stable equilibria and the snap is shown from (4) to (5) as a thick dashed line. The thin dashed line gives the curve of solutions directly below the path from (3) to (4). The point of greatest dorsoventral flexion is denoted by the triangle between points (3) and (4). All units are in radians. (b) A projection of the surface and flexion-snap path onto the $\omega-\alpha$ plane. The value of θ_2 in radians is given by the color bar. (c) Schematic representing the energy landscape for several points along the flexion-snap path. The ball represents the mandible configuration at equilibrium. Step (4) is a point of unstable equilibrium. PE stands for potential energy. (For interpretation of the references to color in this figure legend, the reader is referred to the web version of this article.)

The flexion-snap path begins in the resting position (Fig. 7; point (1)). As before the path proceeds through the following sequence:

(1) → (2), *Twist*: As the model mandible is twisted (ω increasing while α is fixed), the path proceeds until it is beyond the cusp.
(2) → (3), *Rotate*: The mandible is rotated (α decreasing while ω is fixed), allowing the path to transition smoothly to the upper shelf of the surface.
(3) → (4), *Twist back*: Twisting the model back brings the path to a turning point at (4). The maximum angle of flexion is denoted by a triangle.
(4) → (5), *Snap*: The instability of the model results in a sudden jump to a stable configuration. Presumably, much of the energy stored in the hummingbird mandible is converted to kinetic energy while some is lost through damping produced by antagonistic muscular contraction and the surrounding tissue. Twisting back continues until $\omega = 0$.
(5) → (1), *Rotate back*: The model is rotated back until the path returns to the resting position.

The rigid bar model and paper model compare favorably with respect to user controlled inputs and their resulting motion (see Appendix C.3). Since the rigid bar model is discreet, it cannot completely capture the initial curvature of the mandible. However, the flexion angle represents the local deflection away from the initial configuration in the posterior flexion zone, and is consistent with the manner in which the flexion angles were measured in the live specimens. The greatest dorsoventral flexion angle predicted by the model is 23°, which approaches the most extreme values we have yet detected in living birds (27°). These calculations also predict that smaller angels ($\approx 8-22^{\circ}$) leading to snap that can be accessed simply by rotating the mandible less between steps (2) and (3). Lateral mandibular spreading (given by θ_3) is greatest in magnitude near point (3) (11.1°) and just subsequent to point (4) (12.7°). Plots of the angles of rotation and hinge potential energies are shown in Appendix C.3.

6. Anatomical implications

To interpret our mathematical results a detailed understanding of hummingbird cranial anatomy is required. A key challenge is that the muscular activity associated with streptognathism (mandibular bowing) has not been measured directly in any bird. Herein we attempt to present the most plausible mechanism for the observed flexion given hummingbird anatomy and the model results. We draw primarily from our own observations (G.M.Y) and that of Zusi and Bentz (1984) for generalities among hummingbirds. Reviews by Bock (1964, 1999), Bühler (1981), and Zusi (1993) provide a comparative perspective on mediolateral mandibular flexion in birds.

The hummingbird musculoskeletal system is miniaturized and strongly reflects the role of nectar feeding and hovering flight in the evolution and ecology of hummingbirds. The selective pressures associated with nectarivory have resulted in two types of osteological modification: stout load-bearing bones with ample attachment surface for powerful flight muscles (as in the bones of the wing and sternum) and a number of thin, fused bones, e.g. the mandible that are partially rigid and partially flexible. Bones of the latter type are common to the skull and feeding apparatus including an enlarged orbit, a reduced orbital process of the quadrate, and long narrow jaws (Fig. 8). These traits, along with the size and position of the jaw muscles themselves, limit the potential for hummingbirds to generate force while promoting

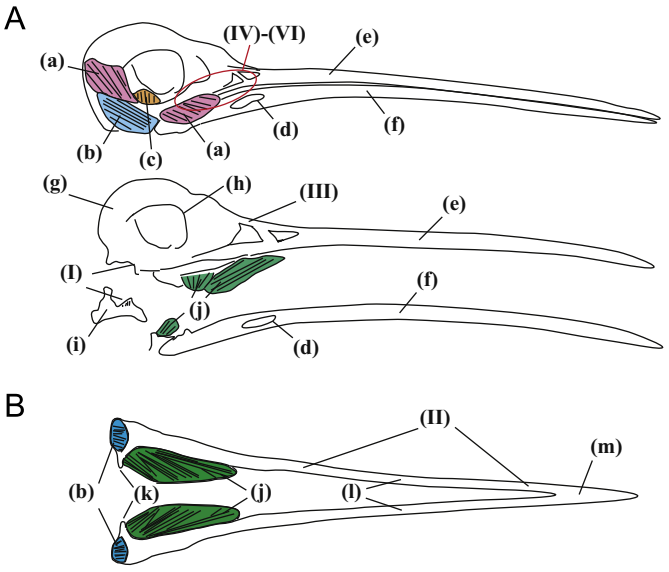

Fig. 8. (A) Generalized lateral hummingbird jaw apparatus. (B) Ventral view of the hummingbird mandible with select muscles. (a) M. adductor mandibulae; (b) M. depressor mandibulae; (c) M. protractor pterygoidei et quadrati; (d) fenestra; (e) maxilla; (f) mandible; (g) braincase; (h) orbital process; (i) quadrate; (j) M. pterygoideus; (k) mandibular condyle or medial process; (l) ramus; (m) symphysis. The roman numerals indicate the flexion zones listed in the text.

the speed of jaw movement and intracranial flexibility (Beecher, 1951; Morioka, 1974; Mayr, 2009). We can identify a number of points on the avian skull that enable intracranial mobility: (I) at the junction of the quadrate, braincase, pterygoid, and jugal bars; (II) at two points along the mandible (the posterior and anterior flexion zones); (III) the upper jaw bends at the craniofacial hinge and near the beak tip (requiring bending from the nasal bar and maxilla); (IV) at the connection of the pterygoids and palate; (V) at the junction of the jugal bars and maxilla; and (VI) at the junction of the palate and the rostrum.

Movement of the mandible is linked to the cranium via paired quadrates and with the upper jaw through the jugal bars, pterygoid–palate complex (points III–VI in the previous paragraph), and the post-orbital ligament. The mandible is lowered when the M. depressor mandibulae (MDM) and M. pterygoidei et quadrati (MPQ) contract (Fig. 8). Contraction of the MPQ moves the quadrate anteromedially, pushing the palate and jugal bars forward and elevating the upper jaw. Meanwhile, contraction of the MDM swings the mandible open like a lever arm around the fulcrum of the quadrates.

Hummingbirds close their jaws through the contraction of two major muscle complexes: the M. pterygoideus and the M. adductor mandibulae (Fig. 8; Bühler, 1981). A primary function of the M. pterygoideus is to retract the palate, thereby lowering the upper jaw. It is worth noting that the M. pterygoideus has multiple parts, with distinct attachment sites and orientations. For example, the M. pterygoideus ventralis medialis (MPVM) originates from the palate and inserts on the medial surface of the mandibular condyle, producing a largely anterior–posterior force vector along the long axis of the beak. The M. pterygoideus ventralis lateralis (MPVL), however, originates at the midline of the palate and inserts lateral to the MPVM, producing a vector of force that is approximately orthogonal to the MPVM. Thus we assume that the MPVM and the MPVL produce the rotation and twist of the mandibular rami, respectively (cf. Zusi, 1962; Zusi and Bentz, 1984; Zusi and Livezey, 2006). The lower jaw is retracted through contraction of M. adductor mandibulae externus pars rostralis lateralis (AMERL)—which originates behind the

eye and inserts on the dorsal and lateral surface of the mandible near the fenestra—and the coordinated relaxation of jaw opening muscles.

The rotation and twist biases of our mechanical model reflect the inferred actions of the muscle groups that open and close the hummingbird's jaws: to date no direct measurements have been made of cranial neuromuscular activity in hummingbirds. The reference configuration in our mathematical model begins with the mandible lowered and the rami twisting outward by the MPQ to some small initial amount. Further outward twisting (i.e., twist bias) is likely produced primarily by the MPVL contraction after the mandible is lowered, and may be partially facilitated by the coordinated displacement of the quadrate and posterior end of the mandible. The posterior end of the mandible is flared both laterally and ventrally. In addition the elongated axis of the mandibular cross section is directed more outward toward the tip, which likely promotes dorsoventral flexion under moderate twist. Therefore, the actual applied twist required may be less than calculated since the model does not precisely capture all of the continuous variations along the mandible. Once the rami are twisted out they are rotated (i.e., rotation bias) via posterior–anterior movement of the mandibular condyle resulting from contraction of the MPVM. This motion rotates the posterior mandibular rami laterally and ventrally, bowing the jaw outward at the posterior flexion zone and inward at the anterior flexion zone (Bühler, 1981; Morioka, 1974).

A critical feature of the proposed flexion-snap process is that the M. pterygoideus muscles (MPVM and MPVL), typically jaw closing muscles, pull antagonistically against the simultaneously contracted MPQ—a protractor of the upper jaw—thereby keeping the jaws apart and under tension. While rotation is held by the antagonism between MPVM and MPQ, the flexed rami are twisted back by the AMERL and approach elastic instability. Thus, when the bird snaps its jaws shut, we propose that the MPQ relaxes, the AMERL twists the rami back to their original position, and the unopposed contraction of the MPVM draws the upper jaw closed. Simultaneously, the mandible tip accelerates via the snap-buckling. Some energy may also be released via elastic recoil in the muscles or tendons of the M. pterygoideus complex. Fig. 9 summarizes the proposed muscular action sequence.

Another result of particular interest predicted by the model is the location, timing, and magnitude of maximum mediolateral mandibular flexion (θ_3) (Fig. 7 and Fig. C2). These values are of particular interest because an increase in the effective width of the gape is expected to enhance the likelihood of prey-capture (Yanega and Rubega, 2004). Given the similarity in foraging styles among swifts (Apodidae), nighthawks (Caprimulgidae), and hummingbirds (Bühler, 1970, 1981), we infer this facet of mandibular flexion to have the greatest historical and functional significance for this clade of highly specialized insectivores. The model indicates that the greatest spreading occurs near the points of maximum twist and rotation bias (3) and also immediately after the snap (4).

Snap-buckling appears to be more energetically costly than simple lateral mandibular flexion (cf. Appendix C.3). However, by coupling lateral spreading and dorsoventral flexion, hummingbirds combine the ability to widen the gape and close the beak quickly with snap-buckling. The increased speed of snap-closure may play a role in feeding performance (Yanega, unpublished data). Ultimately, the speed of jaw closure, the width of the gape prior to the strike and the dorsoventral spread of the beak tips, all features predicted by the model, are likely to combine to augment an individual's ability to successfully catch arthropod prey.

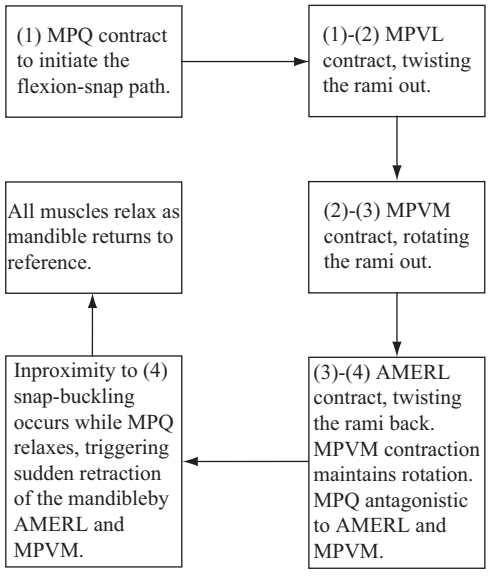

Fig. 9. Summary of proposed muscle action during mandibular flexion and snap. Numbers in the flow chart are consistent with those in Figs. 4 and 7.

7. Summary

We have argued that the rapid closing of the lower humming bird jaw is hard to explain as the result of direct muscular action. The muscles do not seem powerful enough. Rather, the rapid closure might be powered by the sudden release of stored elastic energy. The conclusion is supported first by the unusual construction of the hummingbird lower jaw that has high bending compliance in preferred directions. When we built a paper model that mimics this compliance, we observed it to be capable of an open then snap close mechanism. Further, a more detailed mechanics-based calculation shows similar behavior. Both the paper model and the mathematical calculation use driving forces at the root of the jaw that are consistent with the musculature of the hummingbird. The snap mechanism for closing the jaw is probably more energetically costly to a hummingbird than would be a smooth opening and closing: it involves a loss of kinetic energy at the end of the snap. The benefit, in terms of improved ability to catch insects, presumably outweighs the energetic costs.

Acknowledgments

We are grateful to Diego Sustaita and Margaret Rubega for valuable discussions and a critical review of the manuscript.

Appendix A. Supporting data

The mean maximum dorsoventral flexion angle and mean maximum instantaneous velocity for two typical species are given in Fig. A1(a). This instantaneous tip velocity was calculated from consecutive tip displacement data points ($\Delta x/\Delta t$, where Δx is the change in displacement and Δt is change in time), producing a conservative estimate for the maximum velocity. Representative tip displacement data, from slow opening to rapid closure during one characteristic insect capture event, is shown in Fig. A1(b). Further tip displacement data is being prepared for a future publication. The lower inset in Fig. A1(b) shows only the last 36 ms of the same data set. In order to efficiently calculate tip velocities and accelerations, a sigmoid curve was fit to this data subset. The maximum velocity calculated from this fit was

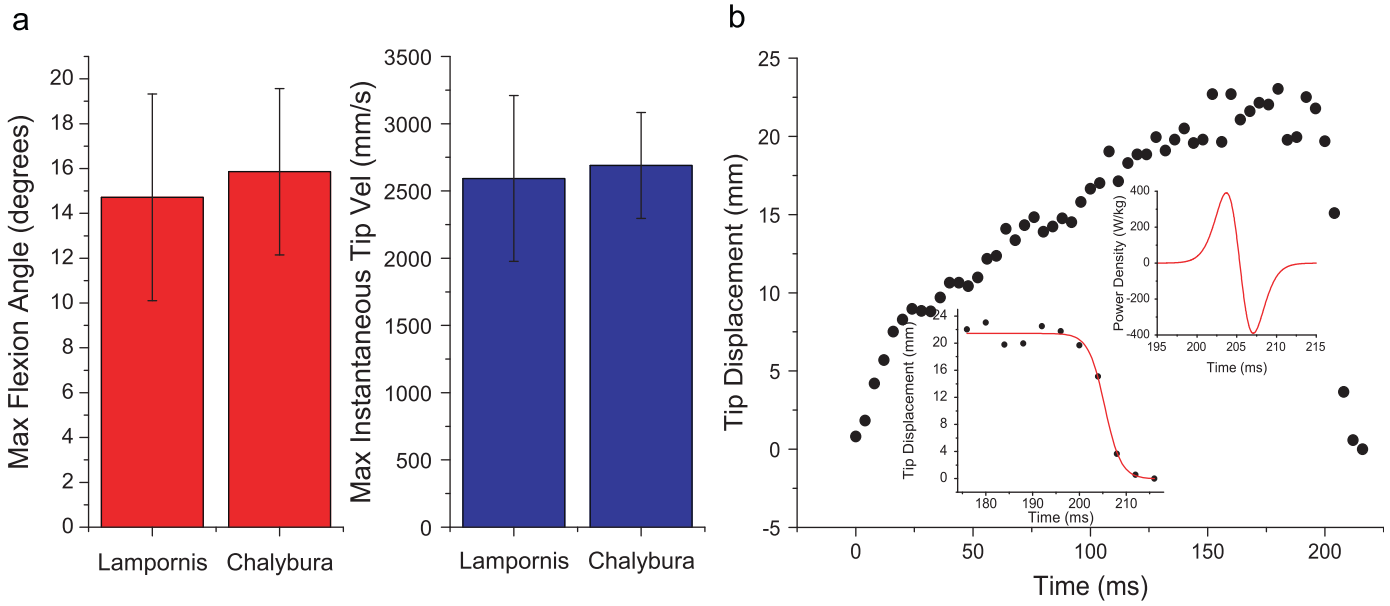

Fig. A1. Beak closure data for hummingbirds. (a) Average maximum dorsoventral flexion angle for blue-throated hummingbirds (*L. clemenciae*) and red-footed plumeleteer hummingbirds (*Chalybura urochyrsia*). (b) Tip displacement during a single representative snap-closure event for a blue-throated hummingbird. Data points (circles) from the last 36 ms are shown with a sigmoid curve fit (lower inset). Calculated power density (power per muscle mass) during rapid closure is shown in the upper inset.

approximately 3000 mm ms^{-1}, which compares reasonably well with the more conservative estimate in Fig. A1(a). The power density (power per muscle mass) is calculated using the tip velocities and accelerations and assumes the mandible is a rigid bar pinned at one end. The mass of half a mandible is approximately 30 mg and we assumed the actuating muscle to have a mass of 39 mg (a 6 mm by 3 mm by 2 mm strip of muscle with density 1.1 g cm^{-3}). Here, the maximum power density is near 390 W kg^{-1} (upper inset Fig. A1b). Using this method power densities over 1000 W kg^{-1} have been calculated. The power output for the flight muscles of hummingbirds is about 310 W kg^{-1}. Available data points during the actual rapid closure are minimal and for this work simplifying assumptions have been made to calculate the power density. Therefore, while this calculation demonstrates the plausibility of elastic snap closure, more detailed investigations are required to definitively prove its existence.

Appendix B. Formulation of the governing equations

The base of the rigid bar model (Fig. 6) is set at the origin of the fixed $\{\hat{\mathbf{i}},\hat{\mathbf{j}},\hat{\mathbf{k}}\}$ basis with the moving bases $\{\mathbf{o}_i\}$, $\{\mathbf{a}_i\}$, and $\{\mathbf{b}_i\}$ at hinges O, A, and B, respectively. The $\{\mathbf{o}_i\}$ basis can be related to the fixed basis in the following way:

$$\mathbf{o}_1=\cos(\theta_3+\phi_3)\hat{\mathbf{i}}+\sin(\theta_3+\phi_3)\hat{\mathbf{j}}$$

$$\mathbf{o}_2=-\sin(\theta_3+\phi_3)\hat{\mathbf{i}}+\cos(\theta_3+\phi_3)\hat{\mathbf{j}}$$

$$\mathbf{o}_3=\hat{\mathbf{k}}, \tag{B.1}$$

Likewise, the other bases are related as follows:

$$\mathbf{a}_1=\mathbf{o}_1,$$

$$\mathbf{a}_2=\cos(\theta_1+\phi_1)\mathbf{o}_2+\sin(\theta_1+\phi_1)\mathbf{o}_3,$$

$$\mathbf{a}_3=-\sin(\theta_1+\phi_1)\mathbf{o}_2+\cos(\theta_1+\phi_1)\mathbf{o}_3, \tag{B.2}$$

and

$$\mathbf{b}_1=\cos(\theta_2+\phi_2)\mathbf{a}_1-\sin(\theta_2+\phi_2)\mathbf{a}_3,$$

$$\mathbf{b}_2=\mathbf{a}_2,$$

$$\mathbf{b}_3=\sin(\theta_2+\phi_2)\mathbf{a}_1+\cos(\theta_2+\phi_2)\mathbf{a}_3. \tag{B.3}$$

Angles θ_1, θ_2, and θ_3 are measured with respect to the reference configuration given by ϕ_1, ϕ_2, and ϕ_3. To simplify notation, let $\vartheta_1=\phi_1+\theta_1$, $\vartheta_2=\phi_2+\theta_2$, and $\vartheta_3=\phi_3+\theta_3$. From Fig. 6 the position of the tip can be written as

$$\mathbf{r}_{OC}=L_{OB}\mathbf{o}_1+L_{BC}\mathbf{b}_1, \tag{B.4}$$

where the length from O to B spans from the base of the jaw to the posterior flexion zone and the length from B to C spans from the posterior flexion zone to the beginning of the beak tip. By Eqs. (A.1)–(A.3), Eq. (B.4) becomes

$$\begin{aligned}\mathbf{r}_{OC}=&[L_{OB}\cos\vartheta_3+L_{BC}\cos\vartheta_2\cos\vartheta_3\\&-L_{BC}\sin\vartheta_1\sin\vartheta_2\sin\vartheta_3]\hat{\mathbf{i}}\\&+[L_{OB}\sin\vartheta_3+L_{BC}\cos\vartheta_2\sin\vartheta_3\\&+L_{BC}\sin\vartheta_1\sin\vartheta_2\cos\vartheta_3]\hat{\mathbf{j}}\\&-L_{BC}\cos\vartheta_1\sin\vartheta_2\hat{\mathbf{k}}.\end{aligned} \tag{B.5}$$

Using the $\hat{\mathbf{j}}$ component from (B.5), the equation for the plane of symmetry is

$$\begin{aligned}0=&-L_{OB}\sin\vartheta_3-L_{BC}\cos\vartheta_2\sin\vartheta_3\\&-L_{BC}\sin\vartheta_1\sin\vartheta_2\cos\vartheta_3+L_{OB}\sin\phi_3\\&+L_{BC}(\cos\phi_2\sin\phi_3+\sin\phi_1\sin\phi_2\cos\phi_3),\end{aligned} \tag{B.6}$$

where the last two terms originate from a point in the plane and we have used the fact that $-\hat{\mathbf{j}}$ is normal to the plane of symmetry. Eq. (B.6) constrains the model tip to the plane of symmetry and we denote the right-hand side as $p(\theta_1,\theta_2,\theta_3)$.

We use static moment balance to derive the equilibrium equations. Taking the model in a deformed configuration we isolate the model from its surroundings at hinges O and C, replacing physical contacts with equivalent forces and moments. By requiring the static moments around the $\hat{\mathbf{k}}$ axis at hinge O to

balance, we obtain

$$\mathcal{K}_3(\alpha-\theta_3)+(\mathbf{r}_{OC}\times-\lambda\hat{\mathbf{j}})\cdot\hat{\mathbf{k}}=0, \tag{B.7}$$

where $\mathcal{K}_3(\alpha-\theta_3)$ is the moment in hinge O due to the torsional spring and $-\lambda\hat{j}$ is the normal force at point C. Likewise, to obtain two more equations, we in turn isolate the model at A and C and then at B and C. We calculate the static moment balance about the $\mathbf{a}_1$-axis and the $\mathbf{b}_2$-axis, respectively, which yields

$$\mathcal{K}_1(\omega-\theta_1)+(\mathbf{r}_{AC}\times-\lambda\hat{\mathbf{j}})\cdot\mathbf{a}_1=0, \tag{B.8}$$

$$-\mathcal{K}_2\theta_2+(\mathbf{r}_{BC}\times-\lambda\hat{\mathbf{j}})\cdot\mathbf{b}_2=0, \tag{B.9}$$

where $\mathcal{K}_1(\omega-\theta_1)$ is the moment in hinge A, $-\mathcal{K}_2\theta_2$ is the moment in hinge B, and $\mathbf{r}_{AC}$ and $\mathbf{r}_{BC}$ can be expanded in a manner similar to $\mathbf{r}_{OC}$ in Eq. (B.5).

Appendix C. Parameter estimates and numerical results

C.1. Reference angles and lengths

We use the reference angles ϕ_1, ϕ_2, and ϕ_3 to adjust the initial orientation of the $\{\mathbf{o}_i\}$, $\{\mathbf{a}_i\}$, and $\{\mathbf{b}_i\}$ bases. Reference angles ϕ_2 and ϕ_3 are obtained from an examination of the ventral side of the cleared skull shown in Fig. C1. For example, a direct measurement of the posterior region gives ϕ_3. The value of ϕ_1 aligns the axis of hinge B with the minimum principal moment of inertia axis of the bone cross section (cf. Fig. 3) in the flexion zone. We measure representative values for L_{OB} and L_{BC} using similar photographs.

C.2. Spring stiffnesses

We assume that the rami are thin enough to keep strains small even though deformations may be large. We also assume deformations characterized by constant curvatures and twists over small estimable lengths. Then it is not hard to relate spring stiffnesses to the mechanical parameters of the continuous mandibular bone. For example, $\mathcal{K}_2=E_2I_{b_2}/L_2$, where L_2 is the length over which the bending anterior to the fenestra occurs and the subscript denotes the value for the Young's modulus (E) and moment of inertia (I_b) based on the location of the bending. The shear modulus (G) is also needed to estimate $\mathcal{K}_1$. The primary unknowns are the moduli and the moments of inertia.

C.2.1. Moments of inertia

We calculate the moments of inertia from simplified composite geometric figures superimposed on bone cross sections. We use cross section 1 in Fig. 3 to calculate the appropriate moment of inertial for hinge B and the polar moment of inertia for hinge A. We use cross section 3 to calculate the moment of inertia for hinge O.

C.2.2. Young's modulus

The mechanical properties of bone are affected by many factors such as porosity, mineral content and collagen fiber orientation (see Martin and Boardman, 1993 and references therein). In particular it has long been established that mineral content correlates closely with Young's modulus (Currey, 1969, 1984). Most often, normal compact bone has a mineral content of 45–85% by mass with a Young's modulus ranging from 4 to 33 GPa in an approximately linear manner (Currey, 1984). It has been observed that the mineral content may be much lower in bones that display extreme flexibility. For example, the anterior portion of the mandible in brown pelicans is made flexible via a reduced area moment of inertia and a low mineral content of approximately 20% (the minimum and maximum values recorded were 15.4% and 23.3%, respectively (Meyers and Myers, 2005)). A second example of bone flexibility is found in the wings of bats. The bone in the wingtip of the Mexican free-tailed bat (*Tadarida brasiliensis*) has no detectable mineral content (Swartz, 1998; Swartz and Middleton, 2008). Swartz (1998) reports elastic modulus levels ranging from 1.3 to 1.8 GPa for these bats.

Like the pelican and the Mexican free-tailed bat, the beak of the hummingbird is much less calcified around and anterior to the posterior flexion zone (see Fig. 1 in Yanega and Rubega (2004)). Direct measurement of the mineral content has not been possible due to the small mass of the hummingbird jaw. Since the flexibility displayed by the hummingbird beak is not unlike that in the brown pelican we assume the mineral content to be lower than the 45% considered in Currey (1984), though perhaps not as low as that found in the wingtips of bats. Therefore, in light of these observations we will use 2 GPa as an estimate for the Young's modulus in the primary flexion zone. For the bone posterior to the fenestra we use 8 GPa since the mineral content is likely much higher.

C.2.3. Shear modulus

Like Young's modulus, the shear modulus also appears to be affected by the bone mineral content. However, studies of the relationship between shear modulus and mineral content are less common. In one available study, Battaglia et al. (2003) determined the effective shear modulus via torsion tests on mouse femurs which had been subjected to various levels of decalcification. The effective shear modulus ranged from 3.7×10^{-1} to 3.46 GPa for mineral contents spanning from 49% to 66%, respectively. Furthermore, Battaglia et al. found the effective shear modulus to be best fit by the power law, $G=10^{-9}x^{6.787}$, where x is the mineral content expressed as a percentage.

It has also been reported that the ratio of Young's modulus to transverse shear modulus for human and bovine cortical bone is on the order of 5:1 (Martin et al., 1998). Whether this ratio would hold for bones with much lower mineral content is unknown. Using the 5:1 ratio we find a shear modulus of 4.0×10^{-1} GPa, which is quite close to the shear modulus measured by Battaglia et al. at 49% mineral content. On the other hand, if we assume the maximum mineral content (23%) found for the brown pelican (Meyers and Myers, 2005), then the power law gives an effective shear modulus of 1.75×10^{-3} GPa. Since the estimates differ by two orders of magnitude an appropriate value for the shear modulus remains in doubt. For a preliminary estimate we set the shear modulus to 5.0×10^{-2} GPa. Initial stiffness estimates before numerical analysis are $\mathcal{K}_1=3.2\times10^{-4}$ N mm, $\mathcal{K}_2=9.6\times10^{-4}$ N mm, and $\mathcal{K}_3=7.5\times10^{-2}$ N mm.

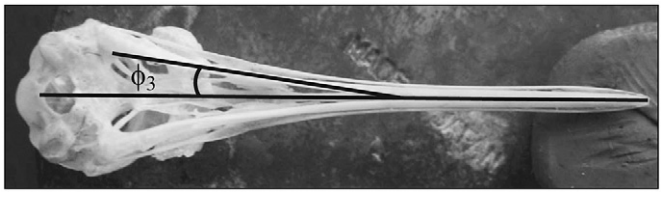

Fig. C1. Ventral view of an intact blue-throated hummingbird skull with measured angle ϕ_3.

C.3. Numerical results

We plot the spring biases, twist (θ_1), flex (θ_2), rotation (θ_3), and potential energies for a complete cycle around the flexion-snap path (Fig. C2). A notable degree of applied twist at the mandible base is required initially (Fig. C2(a) step (2)), but the extreme

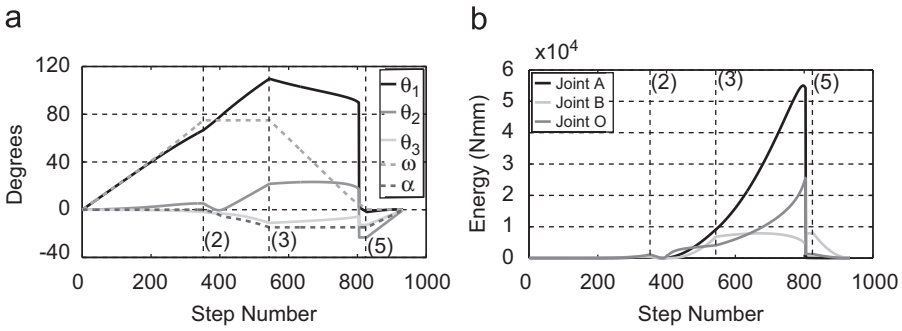

Fig. C2. (a) Plot of twist (θ_1), flex (θ_2), rotation (θ_3), twist bias (ω), and rotation bias (α) for a complete cycle around the flexion-snap path. The horizontal axis represents the step number from the numerical solver. Points on the flexion-snap path where the user switches biases, i.e., (2), (3), and (5) are denoted by dashed vertical lines. (b) Potential energy stored in hinges *A*, *B*, and *O* for a complete cycle around the flexion-snap path. Points on the flexion-snap path where the user switches biases are denoted by dashed vertical lines.

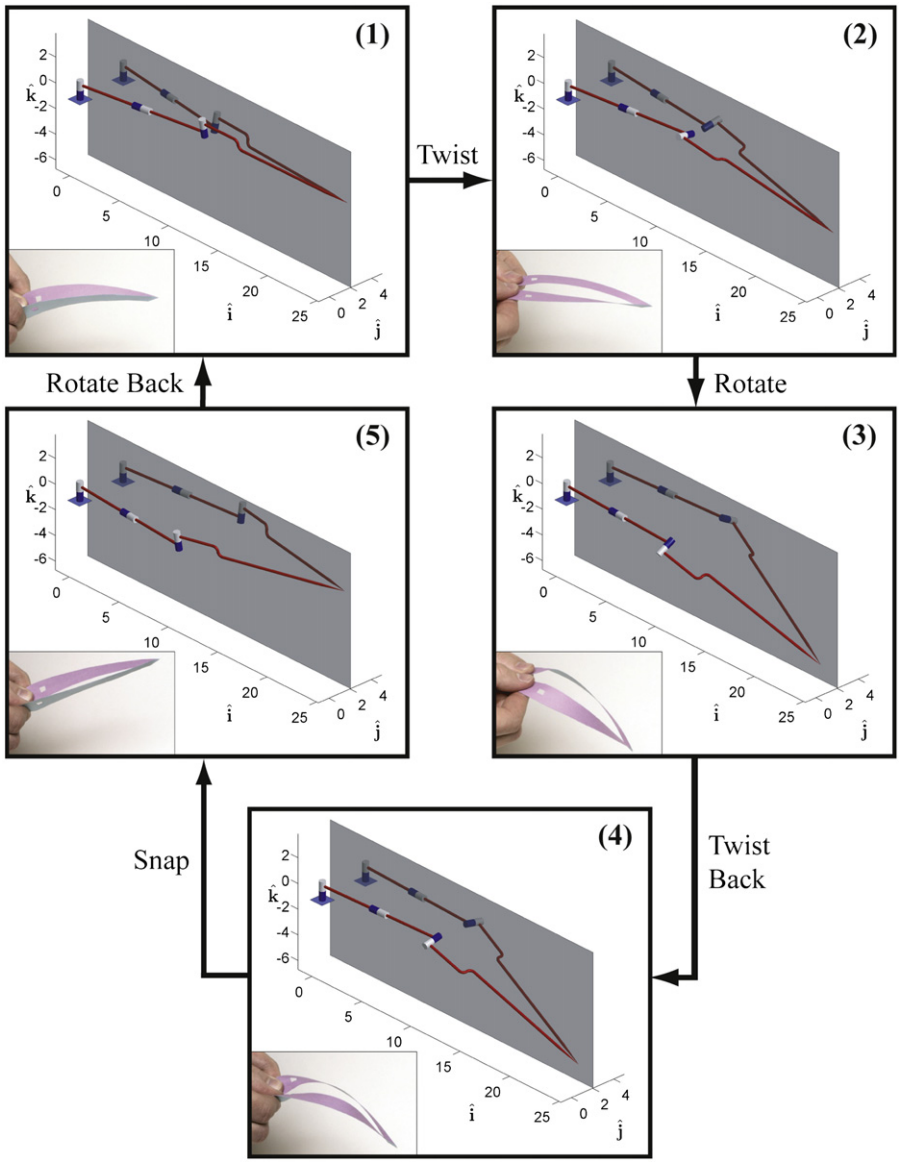

Fig. C3. Configurations of the rigid bar model at stages (1)–(5) on the flexion-snap path. Photographs of the paper model are inset for comparison.

twist seen in step (3) is due in part to twist compliance of the bone itself (ability to twist in the posterior flexion zone). As indicated in Section 6, dorsoventral flexion in hummingbirds likely requires less applied twist due to the continuous variations present in the mandible (particularly cross section elongation becoming more mediolateral toward the mandible tip).

The rotation applied between steps (2) and (3) significantly increases the flex. Then by holding the rotation bias fixed during steps (3) and (4), the twist and flex remain elevated and the potential energy in hinges *A* and *O* increases dramatically. At the same time, the flex reaches its maximum (23°). The mandible snaps from a high energy state to a lower energy state (cf. Fig. 7c), which is indicated by the sharp vertical changes near (5) in Fig. C2.

As a consequence of the snap, the sign of the flex reverses ($\approx -20^\circ$), and the simultaneous jump of the twist to nearly 0° results in simple lateral mandibular flexion (Fig. C3, panel (5)). Lateral mandibular spreading (given by θ_3) is greatest in magnitude near point (3) (11.1°) and just subsequent to point (4) (12.7°). The rigid bar model and paper model compare favorably with respect to user controlled inputs and their resulting motion (Fig. C3).

Appendix D. Supplementary material

Supplementary data associated with this article can be found in the online version of 10.1016/j.jtbi.2011.05.007.

References

Baker, H.G, Baker, I, 1982. Chemical constituents of nectar in relation to pollination mechanisms and phylogeny. In: Nitecki (Ed.), Biochemical Aspects of Evolutionary Biology. University of Chicago Press, pp. 131–171.

Battaglia, T.C., Tsou, A.-C., Taylor, E.A., Mikic, B., 2003. Ash content modulation of torsionally derived effective material properties in cortical mouse bone. J. Biomech. Eng. – Trans. ASME 125, 615–619.

Beecher, W.J., 1951. Adaptations for food-getting in the American blackbirds. Auk 68, 411–440.

Bennet-Clark, H.C., Daws, A.G., 1999. Transduction of mechanical energy into sound energy in the cicada *Cyclochila australasiae*. J. Exp. Biol. 202, 1803–1817.

Bennet-Clark, H.C., Lucey, E.C.A., 1967. The jump of the flea: a study of the energetics and a model of the mechanism. J. Exp. Biol. 47, 59–76.

Bock, W., Kummer, B., 1968. The avian mandible as a structural girder. J. Biomech. 1, 89–96.

Bock, W.J., 1964. Kinetics of the avian skull. J. Morphol. 114, 1–42.

Bock, W.J., 1999. Avian cranial kinesis revisited. Acta Ornithol. 34 (2), 115–122.

Bühler, P., 1970. Schadelmorphologie und kiefermechanik der caprimulgidae aves. Z. Morphol. Tiere 66, 337–399.

Bühler, P., 1981. Functional anatomy of the avian jaw apparatus. In: King, A.S., McLelland, J. (Eds.), Form and Function in Birds, vol. 2. Academic Press (Chapter 8).

Chai, P., Millard, D., 1997. Flight and size constraints: Hovering performance of large hummingbirds under maximal loading. J. Exp. Biol. 200, 2757–2763.

Currey, J., 1969. The mechanical consequences of variation in the mineral content of bone. J. Biomech. 2 (1-A), 1–11.

Currey, J., 1984. Effects of differences in mineralization on the mechanical properties of bone. Philos. Trans. Roy. Soc. B 304 (1121), 509–518.

de Groot, J.H., van Leeuwen, J.L., 2004. Evidence for an elastic projection mechanism in the chameleon tongue. Proc. Roy. Soc. London B Biol. Sci. 271, 761–770.

Forterre, Y., Skothelm, J.M., Dumals, J., Mahadevan, L., 2005. How the venus flytrap snaps. Nature 433, 421–425.

Gibb, A.C., Ferry-Graham, L.A., Hernandez, L.P., Romansco, R., Blanton, J., 2008. Functional significance of intramandibular bending in Poeciliid fishes. Environ. Biol. Fish. 83, 473–485.

Gronenberg, W., 1995. The fast mandible strike in the trap-jaw ant *Odontomachus*: I. temporal properties and morphological characteristics. J. Comp. Physiol. A 176, 391–398.

Hayashi, M., Feilich, K.L., Ellerby, D.J., 2009. The mechanics of explosive seed dispersal in orange jewelweed (*Impatiens capensis*). J. Exp. Bot. 60 (7), 2045–2053.

Lee, M.S.Y., Bell Jr., G.L., Caldwell, M.W., 1999. The origin of snake feeding. Nature 400, 655–660.

Martin, R.B., Boardman, D.L., 1993. The effects of collagen fiber orientation, porosity, density, and mineralization on bovine cortical bone bending properties. J. Biomech. 26 (9), 1047–1054.

Martin, R.B., Burr, D.B., Sharkey, N.A., 1998. Skeletal Tissue Mechanics. Springer-Verlag.

Mayr, G., 2005. A new cypselopmorph bird from the middle eocene of Germany and the early diversification of avian aerial insectivores. Condor 107, 342–352.

Mayr, G., 2009. Phylogenetic relationships of the paraphyletic 'caprimulgiform' birds (nightjars and allies). J. Zool. Syst. Evol. Res. 9999 DOI: 10.1111/j.1439–0469.2009.00552.x.

Meyers, R.A., Myers, R.P., 2005. Mandibular bowing and mineralization in brown pelicans. Condor 107, 445–449.

Morioka, H., 1974. Jaw musculature of swifts (Aves: Apodidae). Bull. Natl Sci. Mus. Tokyo 17 (1), 1–16.

Skals, N., Surlykke, A., 1999. Sound production by abdominal tymbal organs in two moth species: the green silver-line and the scarce silver-line (Noctuoidea: Nolidae: Chloephorinae). J. Exp. Biol. 202, 2937–2949.

Skotheim, J.M., Mahadevan, L., 2005. Physical limits and design principles for plant and fungal movements. Science 308, 1308–1310.

Smith, M.L., 2009. Two problems of mechanics in biology: predicting the onset of DNA supercoiling and modeling mandibular flexion and snap in hummingbirds. Ph.D. Thesis, Cornell University.

Stiles, F.G., 1995. Behavioral, ecological, and morphological correlates of foraging for arthropods by hummingbirds in a tropical wet forest. Condor 97, 853–878.

Suarez, R.K., 1998. Oxygen and the upper limits to animal design and performance. J. Exp. Biol. 201 (8), 1065–1072.

Swartz, S.M., 1998. Skin and bones: functional, architectural, and mechanical differentiation in the bat wing. In: Kunz, T.H., Racey, P.A. (Eds.), Bat Biology and Conservation. Smithsonian Institution Press (Chapter 7).

Swartz, S.M., Middleton, K.M., 2008. Biomechanics of the bat limb skeleton: scaling, material properties and mechanics. Cells Tissues Organs 187, 59–84.

Taylor, P.E., Card, G., House, J., Dickinson, M.H., Flagan, R.C., 2006. High-speed pollen release in the white mulberry tree, *Morus alba* l. Sex Plant Reprod. 19, 19–24.

Temeles, E.J., Kress, W.J., 2003. Adaptation in a plant-hummingbird association. Science 300, 630–633.

Van Wassenbergh, S., Strother, J.A., Flammang, B.E., Ferry-Graham, L.A., Aerts, P., 2008. Extremely fast prey capture in pipefish is powered by elastic recoil. J. Roy. Soc. Interface 5, 285–296.

Yanega, G.M., Rubega, M.A., 2004. Hummingbird jaw bends to aid insect capture. Nature 428, 615.

Young, D., Bennet-Clark, H.C., 1995. The role of the tymbal in cicada sound production. J. Exp. Biol. 198, 1001–1019.

Zack, T.I., Claverie, T., Patek, S.N., 2009. Elastic energy storage in the mantis shrimp's fast predatory strike. J. Exp. Biol. 212, 4002–4009.

Zusi, R.L., 1962. Structural adaptations of the head and neck in the black skimmer. Smithsonian Press.

Zusi, R.L., 1993. Patterns of diversity in the avian skull. In: Hanken, J., Hall, B.K. (Eds.), The Skull: Patterns of Structural and Systematic Diversity. vol. 2. The University of Chicago Press, pp. 391–437.

Zusi, R.L., Bentz, G.D., 1984. Myology of the purple-throated carib (*Eulampis jugularis*) and other hummingbirds (Aves: Trochilidae). Smithson. Contrib. Zool. 385, 1–68.

Zusi, R.L., Livezey, B.C., 2006. Variation in the os palatinum and its structural relation to the palatum osseum of birds (Aves). Ann. Carn. Mus. 75, 137–180.

Zusi, R.L., Warheit, K.I., 1992. On the evolution of intraramal mandibular joints in pseudontorns (aves: Odontopterygia). In: Campbell, J.K.E. (Ed.), Papers in Avian Paleontology Honoring Pierce Brodkorb. Natural History Museum of Los Angeles County, pp. 351–360.

Zweers, G., Berkhoudt, H., VendenBerge, J., 1994. Behavioral mechanisms of avian feeding. In: Bels, V., Chardon, M., Vandewalle, P. (Eds.), Advances in Comparative and Environmental Physiology. Springer-Verlag, pp. 241–279.